N-Acetylgalactosamine-Targeted Delivery of Dendrimer-Doxorubicin Conjugates Influences Doxorubicin Cytotoxicity and Metabolic Profile in Hepatic Cancer Cells

*Sibu P. Kuruvilla, Gopinath Tiruchinapally, Mahmoud ElAzzouny, and Mohamed E. H. ElSayed**

This study describes the development of targeted, doxorubicin (DOX)-loaded generation 5 (G5) polyamidoamine dendrimers able to achieve cell-specific DOX delivery and release into the cytoplasm of hepatic cancer cells. G5 is functionalized with poly(ethylene glycol) (PEG) brushes displaying N-acetylgalactosamine (NAcGal) ligands to target hepatic cancer cells. DOX is attached to G5 through one of two aromatic azo-linkages, L3 or L4, achieving either P1 ($(NAcGal_{\beta}\text{-}PEG_c)_{16.6}$-G5-$(L3\text{-}DOX)_{11.6}$) or P2 ($(NAcGal_{\beta}\text{-}PEG_c)_{16.6}$-G5-$(L4\text{-}DOX)_{13.4}$) conjugates. After confirming the conjugates' biocompatibility, flow cytometry studies show P1/P2 achieve 100% uptake into hepatic cancer cells at 30–60 $\times 10^{-9}$ M particle concentration. This internalization correlates with cytotoxicity against HepG2 cells with 50% inhibitory concentration (IC_{50}) values of 24.8, 1414.0, and 237.8 $\times 10^{-9}$ M for free DOX, P1, and P2, respectively. Differences in cytotoxicity prompted metabolomics analysis to identify the intracellular release behavior of DOX. Results show that P1/P2 release alternative DOX metabolites than free DOX. Stable isotope tracer studies show that the different metabolites induce different effects on metabolic cycles. Namely, free DOX reduces glycolysis and increases fatty acid oxidation, while P1/P2 increase glycolysis, likely as a response to high oxidative stress. Overall, P1/P2 conjugates offer a platform drug delivery technology for improving hepatic cancer therapy.

1. Introduction

Hepatocellular carcinoma (HCC) is the fifth most commonly-occurring cancer worldwide and the second highest cause for cancer-related deaths globally.[1,2] The poor prognosis and treatment of HCC is highlighted by the 782 000 new cases that developed in 2012 and the 746 000 deaths that resulted from it in the same year[2] leading to a global mortality-to-incidence ratio of 0.95.[1–3] In the US, the incidence rate of HCC has more than doubled in the last three decades and is anticipated to reach peak incidence rates before 2030,[4,5] which emphasizes the need to develop an effective therapeutic strategy.

Currently, the most common therapeutic strategy is the direct injection of chemotherapeutic agents (e.g., doxorubicin, DOX) into the hepatic artery through a process called hepatic arterial infusion (HAI).[6] A common modification of this procedure is the co-delivery of an embolizing agent to restrict arterial bloodflow and induce ischemia in addition to the chemotherapeutic effect of DOX, a technique called transarterial chemoembolization (TACE).[7–9] Unfortunately, HAI and TACE are severely hindered by high complication rates such as dose-limiting toxicities (e.g., cardiotoxicity, myelosuppression, and hepatic failure),[10] high rates of tumor recurrence, and development of chemoresistance.[7,11–13] Off-target toxicity arises mainly from the leakage of DOX into the systemic circulation leading to the unintended delivery of DOX to surrounding healthy tissue,[10,14] while chemoresistance develops through upregulation of drug efflux pumps in response to xenobiotic compounds such as DOX.[15]

Our strategy to address the limitations of HAI/TACE and the associated systemic toxicity of the administered chemotherapeutic agent is to engineer a targeted polymer–drug conjugate that can accumulate in the tumor tissue upon parenteral administration, get internalized by hepatic cancer cells via receptor-mediated endocytosis, and achieve selective release of the loaded chemotherapeutic cargo to trigger cancer cell death. Specifically, we utilize generation 5 (G5) of polyamidoamine (PAMAM) dendrimers as the core carrier for DOX

S. P. Kuruvilla
Department of Materials Science and Engineering
University of Michigan
2300 Hayward St., Ann Arbor, MI 48109, USA
Dr. G. Tiruchinapally
Department of Biomedical Engineering
University of Michigan
1101 Beal Avenue, Ann Arbor, MI 48109, USA
Dr. M. ElAzzouny
Department of Internal Medicine
University of Michigan Medical School
1500 East Medical Center Drive
Ann Arbor, MI 48109, USA
Prof. M. E. H. ElSayed
Department of Biomedical Engineering
University of Michigan
1101 Beal Avenue, Ann Arbor, MI 48109, USA
E-mail: melsayed@umich.edu
Prof. M. E. H. ElSayed
Department of Macromolecular Science and Engineering
University of Michigan
2300 Hayward Avenue, Ann Arbor, MI 48109, USA

DOI: 10.1002/adhm.201601046

(as a model chemotherapeutic drug) and *N*-acetylgalactosamine (NAcGal) as a targeting ligand for hepatic cancer cells. G5 polyamidoamine dendrimers are water-soluble, spherical polymers that have 128 terminal amine groups, allowing functionalization of the surface with compounds like drugs, imaging agents, or genetic material.[16,17] We recently reported that G5 dendrimers displaying NAcGal ligands in the beta-conformation ($NAcGal_\beta$) on the end of a 2 kDa poly(ethylene glycol) (PEG) brush and attached to the G5 surface via an acid-labile *cis*-aconitic (*c*) linkage were able to achieve selective internalization into hepatic cancer cells.[18,19] These $NAcGal_\beta$-PEG*c*-G5 conjugates escaped recognition by healthy hepatocytes and liver macrophages[18,19] by targeting the asialoglycoprotein receptor (ASGPR) overexpressed on hepatic cancer cells.[20,21] Upon internalization via receptor-mediated endocytosis, the *cis*-aconityl linkages are hydrolyzed in the acidic endosomes resulting in the shedding of the PEG brush and release of the G5 carrier into the cytoplasm via their endosomolytic activity mediated by the proton sponge effect.[22] We reported the synthesis of aromatic azobenzene linkers that incorporate a 1,6 self-eliminating electron cascade and utilized them to conjugate DOX to G5 dendrimers.[23] These aromatic azobenzene linkers are substrates for azoreductase enzymes expressed by hepatic cancer cells, which mediates cancer cell-specific release of the conjugated cargo.[23] We showed that changing the electron density surrounding the azolinkage [L(x)] by modifying the substituents in *X* and *Y* positions allows us to modulate the affinity to azoreductase enzymes, tune DOX release, and impact the associated cytotoxicity.[23] Namely, the L3 (*X*: N—CH_3; *Y*: H) and L4 (*X*: N—CH_3; *Y*: O—CH_3) linkages exhibited amenable DOX release profiles that correlated with anticancer activity comparable to the toxicity of free DOX in hepatic cancer cells.[23]

In this manuscript, we successfully conjugated DOX to G5 dendrimers via aromatic azolinkers and grafted $NAcGal_\beta$-PEG via acid-labile *cis*-aconityl linkages to prepare two targeted G5-DOX nanoconjugates. We conjugated DOX to G5 dendrimers via L3 and L4 aromatic azolinkers and attached $NAcGal_\beta$-PEG*c* chains to the G5 dendrimers to prepare **P0** $[(NAcGal_\beta\text{-PEG}c)_{12.1}\text{-G5}]$, **P1** $[(NAcGal_\beta\text{-PEG}c)_{16.6}\text{-G5-(L3-DOX)}_{11.6}]$, and **P2** $[(NAcGal_\beta\text{-PEG}c)_{16.6}\text{-G5-(L4-DOX)}_{13.4}]$ (**Figure 1**). We investigated their biocompatibility to determine their potential as an intravenous therapy by quantifying their

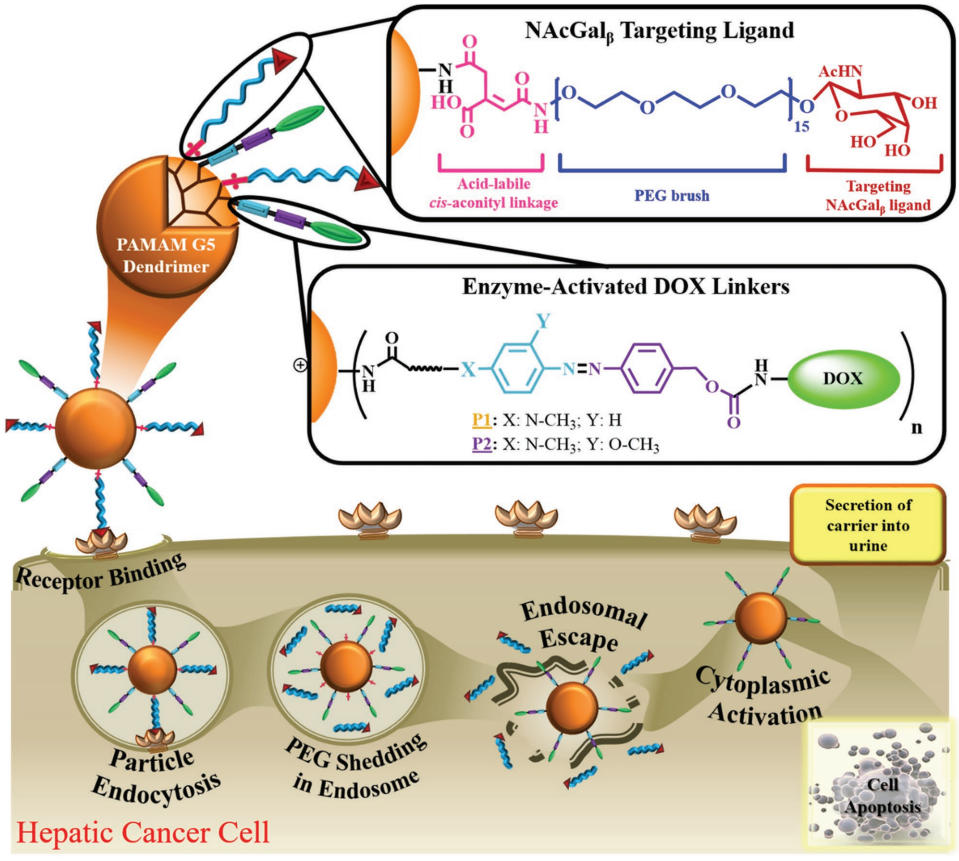

Figure 1. Strategy for targeted, enzyme-activated delivery of doxorubicin to hepatic cancer cells. We functionalized G5 PAMAM dendrimers with *N*-acetylgalactosamine $(NAcGal)_\beta$-terminated PEG brushes attached to G5 via an acid-labile *cis*-aconitic (*c*) spacer to facilitate selective binding to the asialoglycoprotein receptor (ASGPR) overexpressed on hepatic cancer cells. We also attached doxorubicin (DOX) molecules via two different enzyme-sensitive linkages to form either **P1** $[(NAcGal_\beta\text{-PEG}c)_{16.6}\text{-G5-(L3-DOX)}_{11.6}]$ or **P2** $[(NAcGal_\beta\text{-PEG}c)_{16.6}\text{-G5-(L4-DOX)}_{13.4}]$ conjugates. After internalization into the cancer cell via receptor-mediated endocytosis, P1/P2 conjugates shed the $NAcGal_\beta$-PEG*c* branches in the acidic endosome and undergo endosomal escape via the proton sponge effect. In the cytoplasm, the DOX linkages are selectively cleaved by hepatic azoreductase enzymes and release either DOX or DOX-related metabolites that are able to induce tumor cell apoptosis, while the carrier is excreted into the urine.

induction of hemolysis, platelet aggregation, and opsonization by serum proteins. We investigated their uptake by hepatic cancer cells, and the associated anticancer activity compared to free DOX. Prompted by the observed difference in cytotoxicity of free DOX compared to P1 and P2, we employed metabolomics to quantify DOX release and identify the species released from P1 and P2 inside the cytoplasm. This investigation revealed a difference in intracellular species of DOX delivered by the three treatments, as well as a difference in the induced metabolic response (e.g., glycolysis, fatty acid oxidation, and tricarboxylic acid (TCA) cycle), as measured by targeted and untargeted metabolomics approaches. Insights into the efficacy of P1 and P2 conjugates will help evaluate their potential as a platform technology and as an alternative therapy for hepatocellular carcinoma in the clinic.

2. Results and Discussion

2.1. Synthesis and Characterization of P1 and P2 Conjugates

We synthesized G5 dendrimers functionalized with both NAcGal$_\beta$-PEG*c* targeting moieties as well as L(x)-DOX linkages by combining our previous synthetic methodologies[18,23] with minor modifications (**Figure 2**). We confirmed that conjugation of 16.6 NAcGal$_\beta$-PEG*c* units onto G5 surface by NMR and MALDI-TOF (Figure S1, Supporting Information). This corresponds to 13.0 mol% PEGylation of the dendrimer surface, which provides sufficient packing (>5 mol%) to trigger PEG chains to adopt a "brush" conformation instead of the "mushroom" regime.[24,25] This brush conformation enables PEG chains to completely cover the particle's surface and shield it from nonspecific adsorption of serum proteins, which mediates the particle's clearance by the reticuloendothelial system (RES) (i.e., liver, lungs, spleen).[24–26]

The PEGylated G5 (compound **11**) was coupled with L3-DOX or L4-DOX conjugates via click chemistry following published protocols.[23] Starting with the same precursor molecule (compound **11**) ensured equal density of NAcGal targeting ligands per G5 particle before loading of the chemotherapeutic agent (DOX). We achieved similar DOX loading in P1 (compound **12**) [(NAcGal-PEG*c*)$_{16.6}$-G5-(L3-DOX)$_{11.6}$] conjugates and P2 (compound **13**) [(NAcGal-PEG*c*)$_{16.6}$-G5-(L4-DOX)$_{13.4}$] reaching 11.6 moles and 13.4 moles per G5, respectively (Figure 2). We previously established that loading of 16 DOX molecules per G5 (i.e., 12.5% functionalization of surface amine groups) is the maximum capacity to maintain the aqueous solubility of G5-DOX conjugates.[23] Accordingly, P1 and P2 conjugates exhibited intrinsic aqueous solubility at concentrations up to 1.25 mg mL^{-1}.

We measured the size of our conjugates using dynamic light scattering (DLS), identifying that P1 and P2 have hydrodynamic diameters (HD) of 6.02 ± 0.28 nm and 6.39 ± 0.40 nm, respectively (**Table 1**). This size places P1 and P2 conjugates in the ideal size range that will enable them to surpass renal filtration from the blood (HD < 5 nm[27,28]), and thus extends their circulation time within the bloodstream. We also measured the particle size of acetylated G5 (G5-(Ac)$_{128}$) and nonDOX-loaded P0 conjugates to be used as controls (Table 1). We measured the molecular weights of P1 and P2 using MALDI-TOF, which are 84 572 and 85 553 Da, respectively (Table 1; Figures S2 and S3, Supporting Information). This range of MWs places P1 and P2 conjugates well above the molecular weight cut-off of 40 kDa required to escape renal clearance. This MW range also allows them to exploit the enhanced permeation and retention (EPR) effect,[29–32] indicating that during circulation they can extravasate into the tumor interstitium due to its leaky vasculature and be retained there due to the lack of a proper lymphatic drainage system. Finally, we measured the zeta potential of P1 and P2 conjugates which were –0.63 ± 0.28 mV and –0.46 ± 0.23 mV, respectively. The neutral surface charge is important to ensure biocompatibility of PAMAM dendrimers,[33] and also guarantees that the internalization mechanism into cells will not be jeopardized by nonspecific charge–charge interactions.[34]

2.2. Biocompatibility of P1 and P2 Conjugates

We measured the extent of hemolysis induced by P1 and P2 conjugates in the presence of freshly isolated red blood cells (RBCs) by quantifying the amount of released hemoglobin from ruptured RBCs after a 1 h incubation at 37 °C, and compared this behavior to naked, nonPEGylated G5-(NH$_2$)$_{128}$ dendrimers (**Figure 3**, Panel A). Results are presented as a percentage of hemolysis caused by distilled (DI) water, which is considered to cause 100% hemolysis through osmotic swelling and rupture of RBCs.[35] Unmodified G5-(NH$_2$)$_{128}$ dendrimers exhibited complete hemolysis (98.7 ± 3.1%), which can be attributed to membrane destabilization caused by the cationic quaternary ammonium ions that develop at the amine-terminated surfaces of PAMAM dendrimers.[36,37] In comparison, P1 and P2 completely suppressed hemolysis, verifying the established ability of nanoparticle PEGylation[38–40] and neutral surface charge[41] to prevent membrane destabilization and rupture of RBCs.

To ensure both P1 and P2 do not induce platelet aggregation in the bloodstream, we used light transmission aggregometry to measure the activation of platelets in the presence of either particle, following published protocols[42] (Figure 3, Panel B). After drawing fresh blood and isolating the platelet rich plasma (PRP) and platelet poor plasma (PPP) fractions, we added either P1 or P2 to the PRP fraction and compared the resulting aggregation over 10 min to that caused by naked G5-(NH$_2$)$_{128}$ dendrimers or P0 conjugates at an equivalent G5 concentration. Results show that the positive control of adenosine diphosphate (ADP) caused the highest amount of platelet aggregation (26.3 ± 5.36%), which is not surprising due to its established role in platelet activation.[43,44] The effect of PEGylation and surface charge of G5 dendrimers is evident when comparing the 9% platelet aggregation caused by unmodified, cationic G5-(NH$_2$)$_{128}$ dendrimers versus the 0% aggregation caused by the PEGylated P0 particle. Importantly, P1 and P2 conjugates induced no platelet aggregation, indicating that despite the addition of L(x)-DOX molecules (thereby imparting hydrophobicity to the P0 skeleton), PEGylation takes precedence and is able to protect the conjugates from activating platelets.

The advantage of PEGylation and its precedence over the addition of hydrophobic L(x)-DOX linkages is further evident in the opsonization of P1 and P2 conjugates. Opsonization, or the

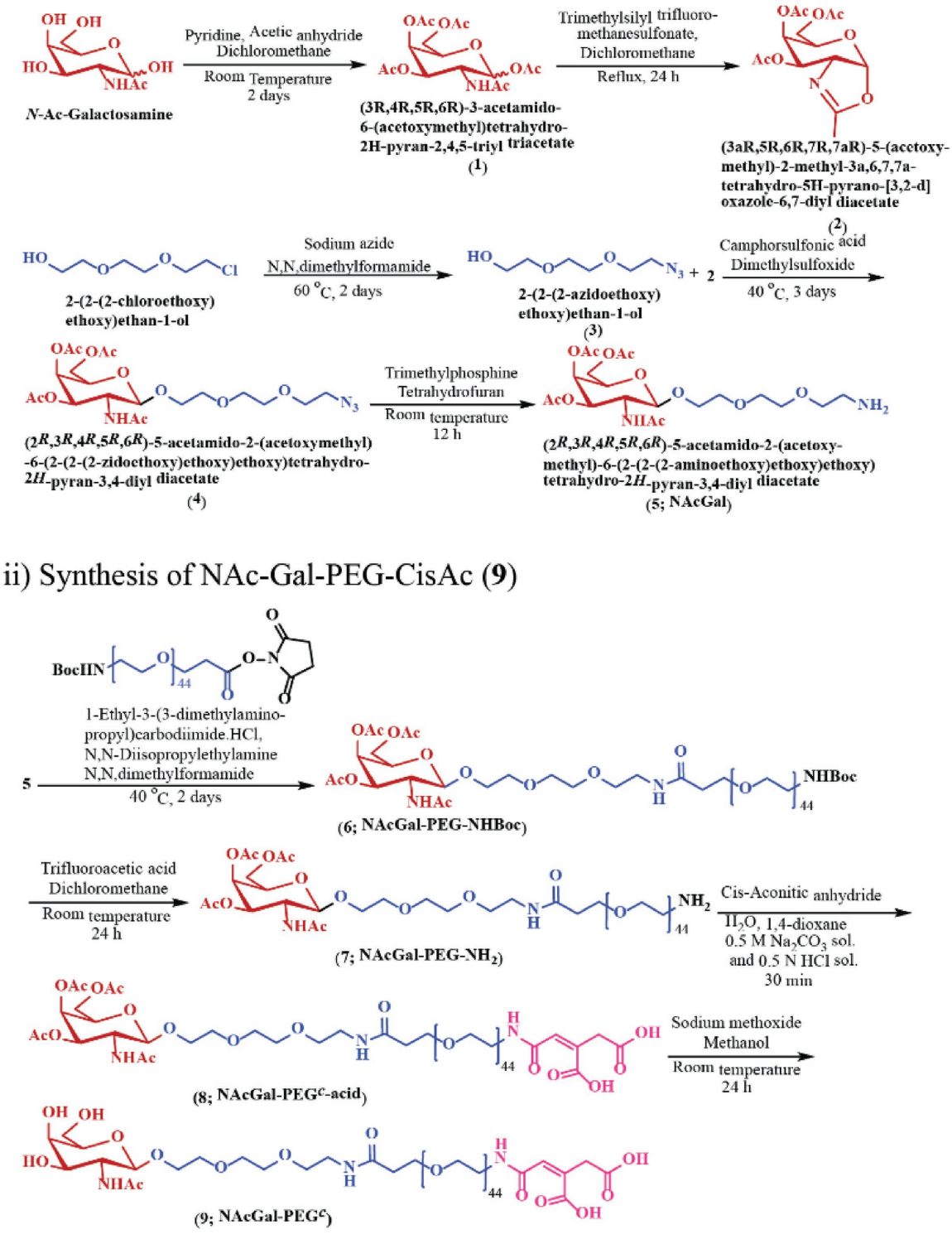

Figure 2. Synthesis of P1 and P2 conjugates. To achieve NAcGal$_\beta$-targeted, DOX-loaded nanoconjugates we first functionalized the G5 surface with 16.6 moles of NAcGal$_\beta$-targeted PEG brushes attached via an acid-labile *cis*-aconitic linkage. We then loaded either 11.6 moles of L3-DOX molecules or 13.4 moles of L4-DOX molecules via click-coupling to achieve P1 and P2, respectively. P1 and P2 conjugates have hydrodynamic diameters of 6.02 and 6.39 nm, respectively, and molecular weights of 84 572 or 85 533 Da.

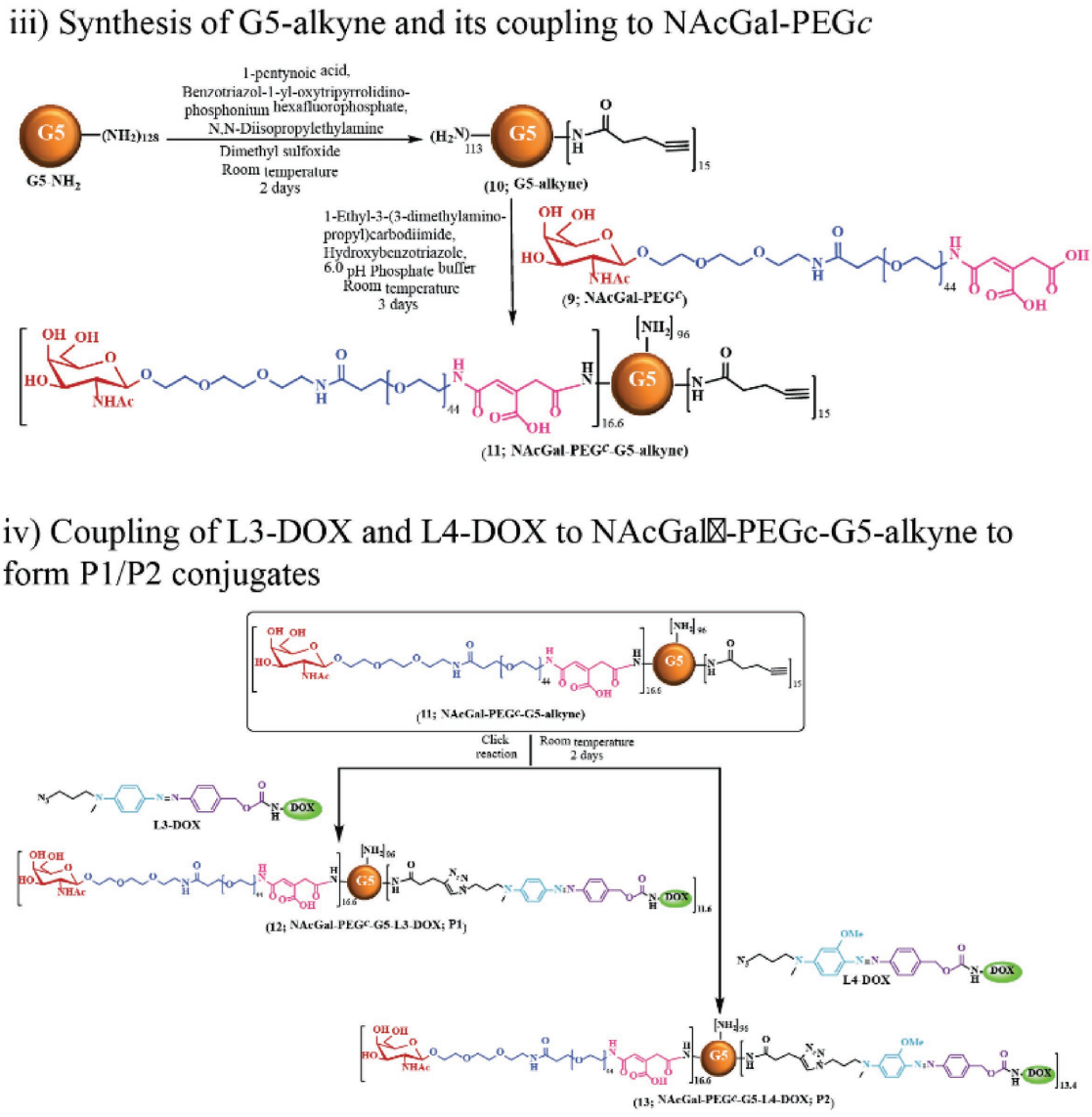

Figure 2. Continued.

fouling of a surface by nonspecific protein adsorption during plasma circulation, leads to rapid shuttling of nanoparticles to organs of the RES within minutes of intravenous delivery. As such, opsonization is one of the largest barriers facing nanomedicine strategies.[45–47] To approximate the extent of opsonization of our NP formulations, we measured the binding of bovine serum albumin (BSA) to their surfaces using the change in intrinsic fluorescence of BSA, which is quenched when the protein binds to the NP surface.[18] In particular, we investigated the adsorption of BSA to P1 and P2 conjugates in comparison to G5-$(NH_2)_{128}$ dendrimers and P0 conjugates at equal G5 concentration (Figure 3, Panel C). Results show that the fluorescence intensity of free BSA remained relatively unchanged during the 60 min incubation period and thus was used as the negative control. Cationic, G5-$(NH_2)_{128}$ dendrimers exhibit high (four- to sevenfold) fluorescence quenching, reaching an I^0/I value of 7.18 ± 1.90 at the end of the incubation period. This is expected given the high surface charge of the particle due to the 128 free terminal amines on its surface. In comparison, P0 conjugates exhibit no fluorescence quenching, which is not surprising given its neutral surface charge imparted by

Table 1. Physicochemical properties of G5-based conjugates.

Particle name	Chemical composition	MW [Da]	Particle size [nm]	Zeta potential [mV]
G5-$(Ac)_{128}$	G5-$(Ac)_{128}$	34 200	5.59 ± 0.56	1.22 ± 1.44
P0	$(NAcGal_{\beta}\text{-}PEGc)_{12.1}$-G5	59 171	7.43 ± 0.34	−0.30 ± 0.21
P1	$(NAcGal_{\beta}\text{-}PEGc)_{16.6}$-G5-$(L3\text{-}DOX)_{11.6}$	84 572	6.02 ± 0.28	−0.63 ± 0.28
P2	$(NAcGal_{\beta}\text{-}PEGc)_{16.6}$-G5-$(L4\text{-}DOX)_{13.4}$	85 533	6.39 ± 0.40	−0.46 ± 0.23

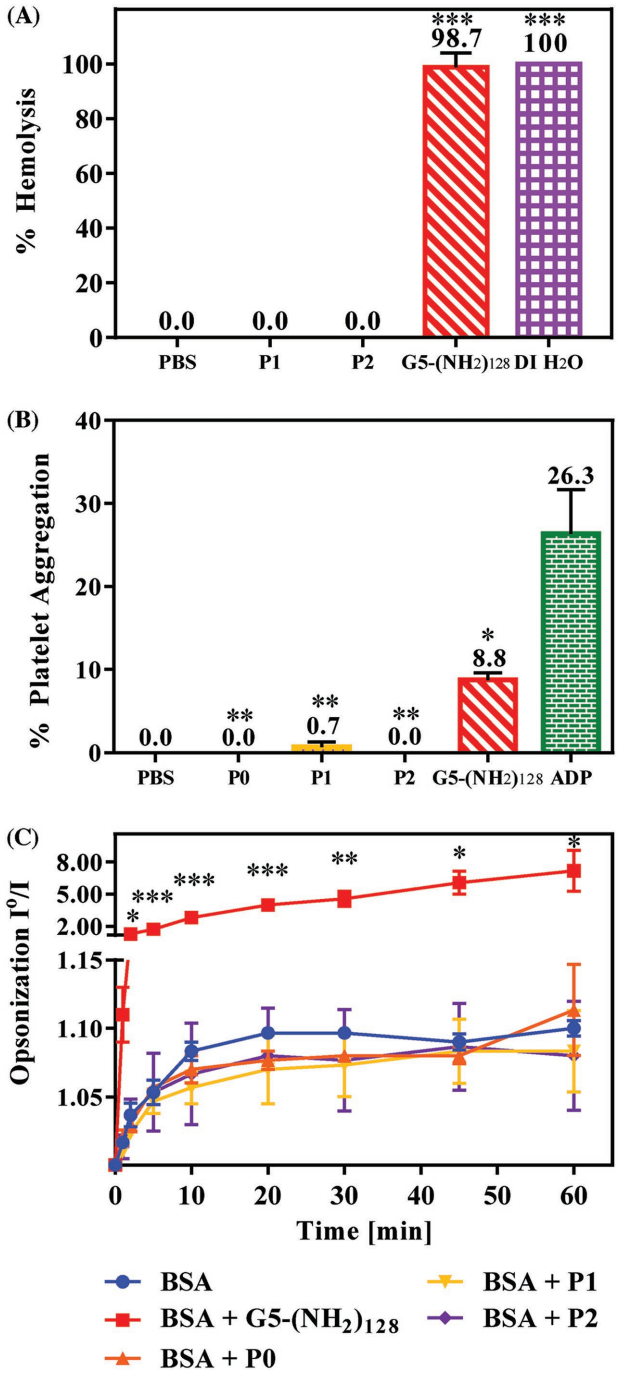

Figure 3. Biocompatibility of P1 and P2 conjugates. We evaluated the biocompatibility of P1 and P2 conjugates by A) measuring the extent of hemolysis, B) platelet aggregation, and C) opsonization by serum proteins. Results show that P1 and P2 do not induce hemolysis in red blood cells compared to PBS controls (A), and they also do not cause aggregation of platelets (B). Further, opsonization studies show that P1 and P2 are able to escape recognition by serum proteins due to their neutral charge and PEG corona (C). Results are presented as the means of at least three replicates ± SEM. Two-tailed Student's t-tests were used to determine the statistical difference between each treatment and the positive control of the respective study (DI H_20, ADP, or G5-$(NH_2)_{128}$, respectively), which is denoted by * for $P < 0.05$, ** for $P < 0.01$, and *** for $P < 0.001$.

the capping (acetylation) of the free amine groups as well as the hydrophilic nature of the PEG that is able to prevent protein adsorption to the particle surface.[18] As mentioned, neither P1 nor P2 conjugates exhibited any fluorescence quenching, suggesting that they are able to escape recognition by serum proteins. Moreover, P1 and P2 conjugates have free amines that are not acetylated nor functionalized, yet the 16.6 moles of 2 kDa PEG chains with hydrophilic NAcGal$_\beta$ ligands are able to cover their surfaces and mask them from protein recognition.

Taken together, the high in vitro biocompatibility observed in these results validates the utility of PEGylation, water-soluble polymers, neutral surface charge, and functionalization with hydrophilic NAcGal$_\beta$ targeting ligands for intravenous drug delivery systems. Results suggest that P1 and P2 conjugates will be able to overcome rapid clearance from the bloodstream and can be retained long enough in circulation to exploit the EPR effect and achieve high intratumoral concentrations, all while causing minimal adverse effects to blood components.

2.3. Uptake of P1 and P2 Conjugates into Hepatic Cancer Cells

We were interested to see if the addition of L(x)-DOX molecules to NAcGal$_\beta$-targeted, PEGylated G5 dendrimers would be able to retain affinity for hepatic cancer cells. Therefore, we measured the internalization of P1 and P2 conjugates into HepG2 or Hep3B cells over 2 and 24 h as a function of concentration via flow cytometry. We previously established that the ideal concentration range of NAcGal$_\beta$ ligands is 10–4000 × 10^{-9} M in order to achieve controllable labeling and internalization of G5-based conjugates into HepG2 and Hep3B cells.[18] Therefore, we incubated P1 and P2 conjugates over this NAcGal$_\beta$ concentration range, which is equal to 0.6–240 × 10^{-9} M of P1/P2 conjugates. We used the intrinsic fluorescence of DOX to measure the number of cells labeled by P1/P2 conjugates and we included equivalent concentrations of free DOX to compare the internalization of free DOX to that delivered by G5 carriers. It is important to note that we accounted for the slight difference in DOX-loading in P1 and P2 by adjusting the concentration of free DOX used in uptake studies to allow accurate assessment of the particle's internalization (**Figure 4**).

Results show P1 and P2 conjugates are internalized into hepatic cancer cells in a concentration-dependent manner, which is higher than the internalization of equivalent concentrations of free DOX (Figure 4, Panels A and C). In HepG2 cells, at an NAcGal$_\beta$ concentration of 100 × 10^{-9} M, P1 conjugates fluorescently label 14% of cells and P2 conjugates label 39% (Figure 4, Panel A). Free DOX, on the other hand, at both equivalent concentrations (46 × 10^{-9} M DOX for P1, or 61 × 10^{-9} M for P2) only labels 2% of HepG2 cells. As the NAcGal$_\beta$ concentration increased to 500 × 10^{-9} M, P2 conjugates virtually label all cells, while free DOX only labels 2%. Similarly, P1 reaches 97% labeling of cells at a NAcGal$_\beta$ concentration of 1000 × 10^{-9} M, while the equivalent incubation of free DOX only labels 43% of cells. At the highest concentration of 4000 × 10^{-9} M, all formulations reach 100% cell labeling. Similarly, P1 conjugates fluorescently labeled up to 12-fold more Hep3B cells than free DOX and P2 labeled up to 78-fold more cells (Figure 4, Panel C). We also investigated the uptake of P1 and P2 conjugates into

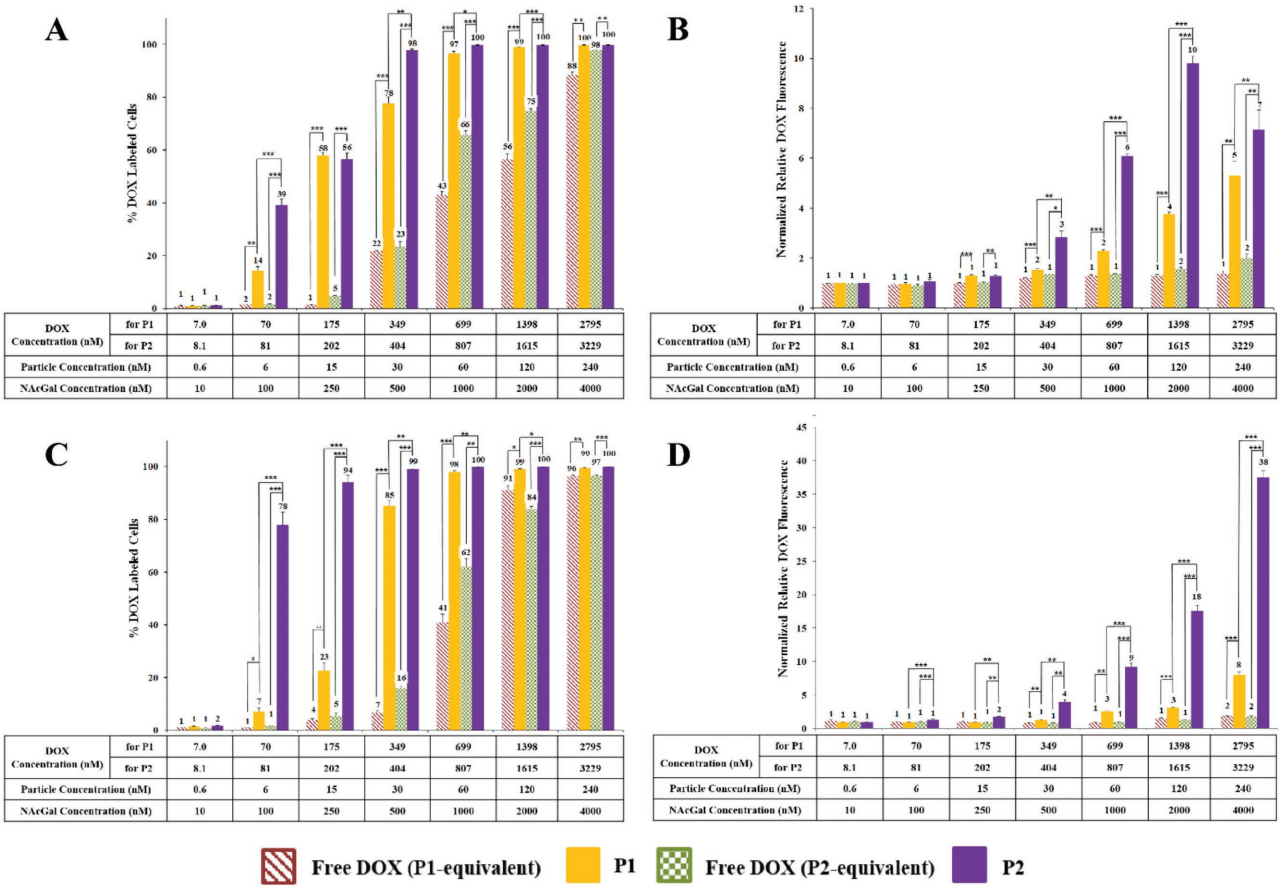

DOX Concentration (nM)								
	for P1	7.0	70	175	349	699	1398	2795
	for P2	8.1	81	202	404	807	1615	3229
Particle Concentration (nM)		0.6	6	15	30	60	120	240
NAcGal Concentration (nM)		10	100	250	500	1000	2000	4000

Figure 4. Uptake of P1 and P2 conjugates into HepG2 and Hep3B cells. We measured the internalization of P1 and P2 conjugates into hepatic cancer cells in comparison to free DOX via flow cytometry. P1 and P2 were incubated at NAcGal concentrations of 10–4000 × 10^{-9} M for 2 h at 37 °C, and their equivalent DOX-loaded concentrations were used for free DOX incubations, as shown in the Table. Results show that both P1 and P2 label a significantly higher number of cells than their free DOX counterparts (A,C), and this leads to as high as a 38-fold increase in intracellular fluorescence (B,D). Results are presented as the means of three replicates ± SEM. Two-tailed Student's t-tests were used to determine the statistical difference between each treatment and is denoted by * for $P < 0.05$, ** for $P < 0.01$, and *** for $P < 0.001$.

a control cell line, SK-Hep1, which is ASGPR-deficient.[48–50] Results show that these cells do not bind or internalize P1/P2 conjugates, demonstrating that uptake of the conjugates into HepG2 and Hep3B cells is ASGPR-mediated (Figure S4, Supporting Information). Further, we normalized the relative fluorescence intensity of fluorescently labeled HepG2 and Hep3B cells to that of untreated cells in order to measure the difference of intracellular DOX concentration between different formulations (Figure 4, Panels B and D).[18,51,52] P1 and P2 conjugates achieved up to sixfold increase in intracellular DOX concentration over the free drug incubation in HepG2 cells (Figure 4, Panel B). In Hep3B cells, P1 achieved up to fourfold increase over free DOX while P2 achieved a 19-fold increase at the highest particle concentration (Figure 4, Panel D).

These results indicate that the higher fluorescent labeling and intracellular fluorescence of DOX mediated by P1 and P2 conjugates in both HepG2 and Hep3B cells highlight the advantage of active targeting through $NAcGal_{\beta}$-facilitated receptor-mediated endocytosis. We previously established that the display of $NAcGal_{\beta}$ ligands at the end of a PEG brush was able to achieve selective internalization of G5 dendrimers into hepatic cancer cells, and escaped recognition by nontarget cells, namely healthy hepatocytes and liver macrophages (i.e., Kupffer cells).[18] It is evident that P1 and P2 conjugates maintain uptake capability into hepatic cancer cells, despite the addition of L(x)-DOX molecules, and in terms of percentage of cells labeled and intracellular DOX fluorescence, they exhibit a clear advantage over passive diffusion of free DOX. In addition, it is important to note that P1 and P2 conjugates exhibit higher cell labeling and higher intracellular concentration in Hep3B cells than HepG2 cells almost universally, achieving a maximum of 5.4-fold higher intracellular fluorescence for P2 conjugates at the same concentration (Figure 4, Panels B and D). We attribute this differential to the variation in expression of ASGPR between cell lines, which has been confirmed to be greater for Hep3B cells than in HepG2 cells.[20,53,54]

2.4. Cytotoxic Activity of P1 and P2 Conjugates

We incubated free DOX, P1, and P2 conjugates with HepG2 and Hep3B cells over 72 h and used the clonogenic survival

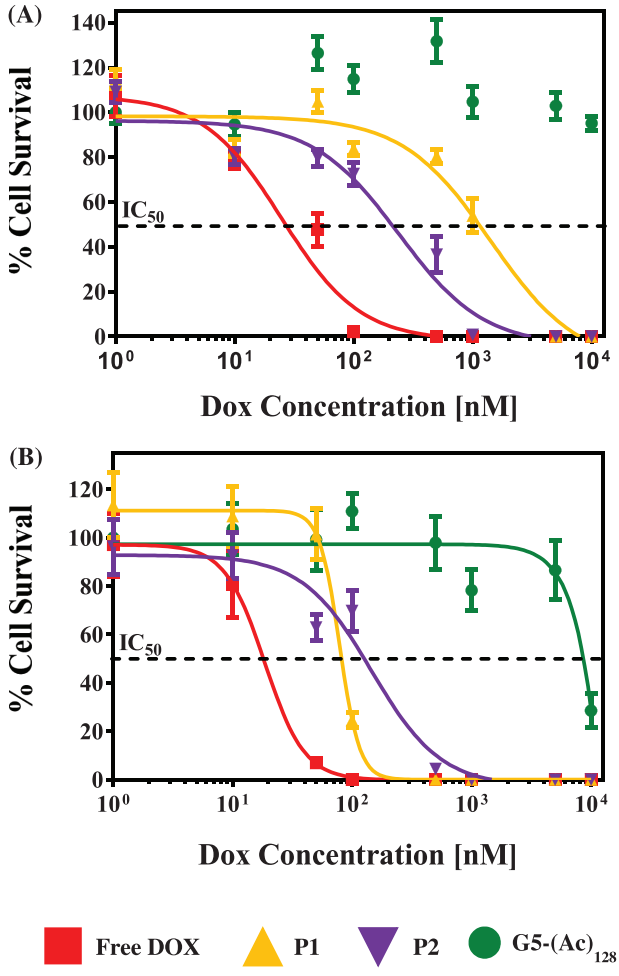

Figure 5. Anticancer activity of P1 and P2 conjugates against HepG2 and Hep3B cells. We measured the cytotoxicity profiles of P1 and P2 compared to free DOX against hepatic cancer cells after a 72 h treatment via the clonogenic survival assay. Results show that in HepG2 cells (A), free DOX, P1, and P2 exhibit IC_{50} values of 24.8 ± 1.19 × 10^{-9} M, 1414.0 ± 1.42 × 10^{-9} M, and 237.8 ± 1.20 × 10^{-9} M, respectively. In Hep3B cells (B), IC_{50} values were 18.6 ± 1.26 × 10^{-9} M, 78.5 ± 1.1 × 10^{-9} M, 145.5 ± 1.3 × 10^{-9} M, respectively. The non DOX-loaded P0 carrier showed no (≥10 000 × 10^{-9} M) toxicity in either cell line. Results are presented as the means of three replicates ± SEM.

assay to measure cell survival following our published protocols.[23] As expected, free DOX induced an exponential decrease in HepG2 cell survival with increasing DOX concentration, achieving an IC_{50} (median concentration of drug required to inhibit cell growth by 50%) of 24.8 ± 1.2 × 10^{-9} M (**Figure 5**, Panel A). This IC_{50} is comparable to our established results and falls in the expected range of DOX toxicity in HepG2 cells for these treatment conditions.[55,56] We measured the intrinsic toxicity of P0 and results show that it has insignificant toxicity within the investigated concentration range with IC_{50} > 10 000 × 10^{-9} M (Figure 5, Panel A). P1 and P2 conjugates exhibited increasing toxicity with increasing DOX concentration achieving IC_{50} values of 1414.0 ± 1.4 × 10^{-9} M and 237.8 ± 1.2 × 10^{-9} M, respectively (Figure 5, Panel A). It is evident that P2 has a higher activity than P1 indicated by its IC_{50} value that is sixfold lower than that of P1. This is expected given that it has 1.8 more DOX moles/G5 carrier and the higher affinity for azoreductase enzymes responsible for cleavage of the linkage and release of DOX as established in previous reports.[23] Results in Hep3B cells follow similar trends (Figure 5, Panel B) with toxicity increasing exponentially with DOX concentration, while the carrier P0 again shows insignificant toxicity with an IC_{50} ≈ 10 000 × 10^{-9} M (Figure 5, Panel B). Consistent with previous results,[23,55] Hep3B cells are more sensitive to treatment than HepG2 cells, with free DOX, P1, and P2 having lower IC_{50} values of 18.6 ± 1.3 × 10^{-9} M, 78.5 ± 1.1 × 10^{-9} M, and 145.5 ± 1.25 × 10^{-9} M, respectively. In addition to the higher intrinsic sensitivity to treatment, our internalization results (Figure 4, Panels B and D) also showed that P1 and P2 conjugates achieve higher intracellular concentrations in Hep3B over HepG2 cells, and thus higher intracellular DOX concentrations may be contributing to the higher toxicity. Further, similar to what we observed in our previous results,[23] P1 particles are more cytotoxic than P2 particles in Hep3B cells. We hypothesize that this variation may be attributed to differences in azoreductase identity and expression between cell lines, but further studies are required to test this hypothesis. Nevertheless, these results verify that P1 and P2 conjugates are able to exhibit toxicity toward hepatic cancer cells that is comparable to free DOX and this toxicity can be optimized by tuning linkage composition.

2.5. Intracellular Release of DOX from P1 and P2 Conjugates via Metabolomics Studies

The differences in cytotoxicity between free DOX, P1, and P2 particles prompted us to elucidate the intracellular fate of DOX being delivered by each treatment. We employed metabolomics to determine the chemical fingerprints of DOX delivered by P1 and P2 conjugates intracellularly in comparison to DOX delivered freely in solution. We chose a treatment time of 12 h to provide a snapshot of metabolic alteration induced by the DOX-loaded conjugates without causing substantial cell death commonly observed after 24 h.[57,58] Both intracellular and extracellular metabolites were analyzed by liquid chromatography-mass spectrometry (LC-MS) (**Figure 6**). Results show that treatment of HepG2 cells for 12 h with free DOX results in detection of the parent DOX ($[M-H]^-$: 542.1710) and 7-deoxydoxorubicinone ($[M-H]^-$: 395.0587), which is its deglycosylated form (Figure 6, Panel A). This conversion has been shown to be mediated by a combination of cytochrome P450s and nicotinamide adenine dinucleotide-hydrogen (NADH) dehydrogenase,[59,60] which are both cytosolic enzymes.

Although P1 and P2 conjugates exhibited significant cytotoxicity toward HepG2 cells (Figure 5), results show a significantly lower amount of the parent DOX present intracellularly from these treatments (Figure 6, Panel A). This can be attributed to slow release of DOX molecules from P1 and P2 conjugates, which dramatically minimized intracellular concentration of parent DOX at this 12 h time point. Using untargeted metabolomics, we found both P1 and P2 conjugates generated two specific molecules that are structurally similar to the

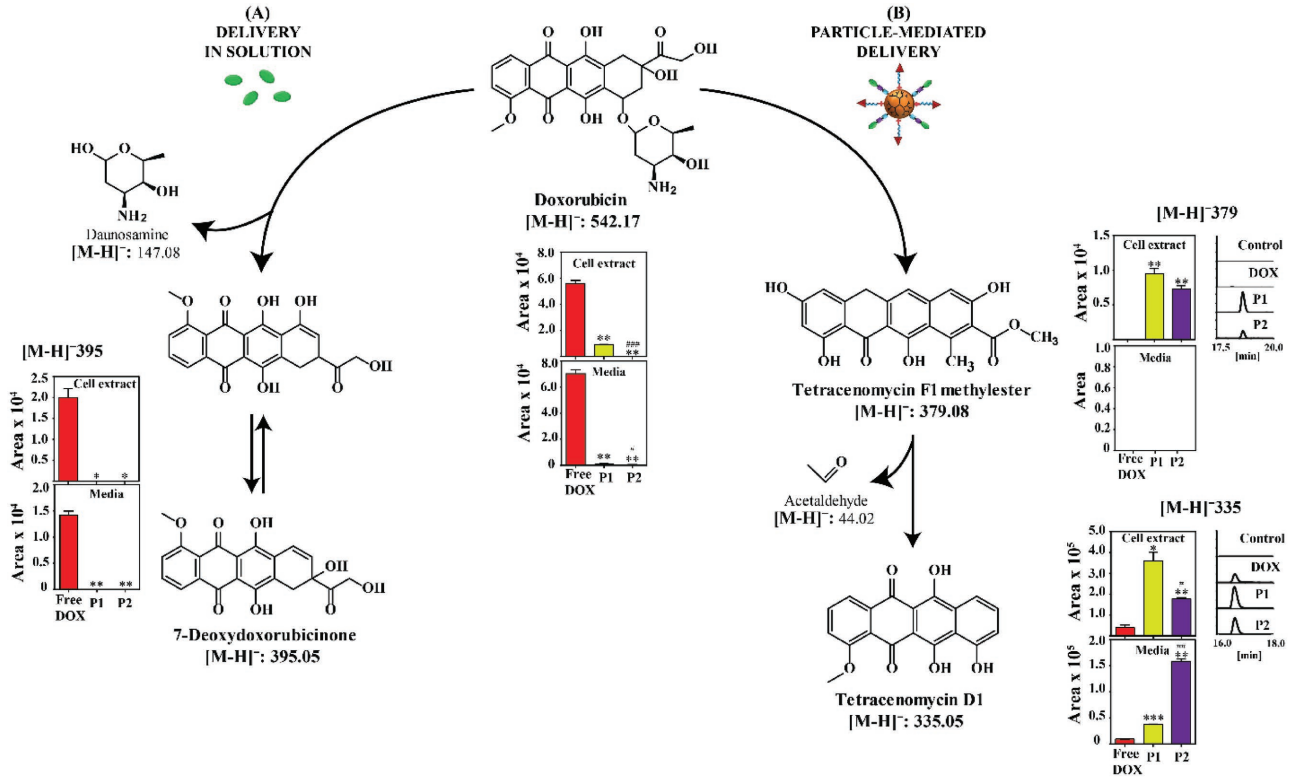

Figure 6. Metabolomics identifies different DOX-related metabolites delivered by P1 and P2 conjugates. We employed metabolomics to determine the chemical fingerprints of DOX delivered by P1 and P2 conjugates in comparison to DOX delivered freely in solution after a 12 h treatment of HepG2 cells. A) Results show that free DOX generates two different metabolites: parent DOX ([M–H]⁻: 542.1710) and its deglycosylated form, 7-deoxydoxorubicinone ([M–H]⁻: 395.0587). B) P1 and P2 conjugates deliver other DOX-related metabolites, namely tetracenomycin analogs F1 methylester ([M–H]⁻: 379.0823) and D1 ([M–H]⁻: 335.0561). Intracellular and extracellular abundance of each metabolite is presented as the mean of three replicates ± SEM. Two-tailed Student's t-tests were used to determine the statistical difference between P1 or P2 compared to free DOX (*) or between P1 and P2 (#), and are denoted by * or # for $P < 0.05$, ** or ## for $P < 0.01$, and *** or ### for $P < 0.001$.

anthracycline backbone of DOX but only one that matched the exact mass ([M–H]⁻: 335.0561) of a known DOX metabolite recently described by Kaushik and Bansal.[61] (Figure 6, Panel B). These molecules are similar in exact mass to tetracenomycin (TCM) compounds, which are structural isomers of DOX metabolites[61] that are known to exhibit similar cytotoxicity via DNA intercalation, topoisomerase II inhibition, and generation of reactive oxygen species (ROS).[62–64] Therefore, we chose TCM nomenclature to identify these metabolites. However, it is important to note that TCM compounds are less potent than the parent DOX, which is indicated by their higher IC_{50} values.[63] For example, Gan et al. reported an IC_{50} of 7.5×10^{-6} M for TCM X in HepG2 cells compared to an IC_{50} of 1.6×10^{-6} M for DOX.[63] The TCM F1 methylester analogue ([M–H]⁻: 379.0823) appeared in the intracellular extracts of P1- and P2-treated cells at similar quantities (Figure 6, Panel B), which indicates that this metabolite is generated from the P1/P2 conjugates by intracellular enzymes. The second and most prominent metabolite identified from P1- ad P2-treated cells is TCM D1 ([M–H]⁻: 335.0561), which results from the loss of an acetaldehyde group from TCM F1 methylester (Figure 6, Panel B). Free DOX treatments also generated the TCM D1 metabolite, which is not surprising given that it is a downstream metabolite of parent DOX after the loss of a glycolaldehyde group from 7-deoxydoxorubicinone.[61] However, the quantity of intracellular TCM D1 in free DOX-treated cells, is nine- and fourfold lower than that observed in P1 ($P < 0.05$) and P2 ($P < 0.01$) treated cells, respectively (Figure 6, Panel B). Interestingly, the levels of TCM D1 inside HepG2 cells are significantly higher for P1 treated cells compared to those incubated with P2 ($P < 0.05$) while the extracellular concentration of the same metabolite is reversed (i.e., higher for P2 than P1, $P < 0.01$). It is also important to note that TCM D1 molecules were generated when P1 and P2 conjugates were incubated with phosphate buffered saline (PBS) alone (data not shown), albeit at lower levels than those detected inside HepG2 cells. This suggests that introducing the drug with a nanoparticle might force it to undergo special chemical modifications that could exert toxic effects on its own. Additionally, since it is also common to see nonspecific degradation pathways for free DOX molecules in buffers,[65] it is possible that P1 and P2 conjugates are not completely devoid of this degradation either.

The exact mechanism of intracellular release and metabolism of DOX delivered by P1 and P2 conjugates that result in generation of TCM F1 and D1 molecules is still unclear. Earlier reports show that changing the enzyme responsible for releasing a therapeutic cargo from a polymer–drug conjugate

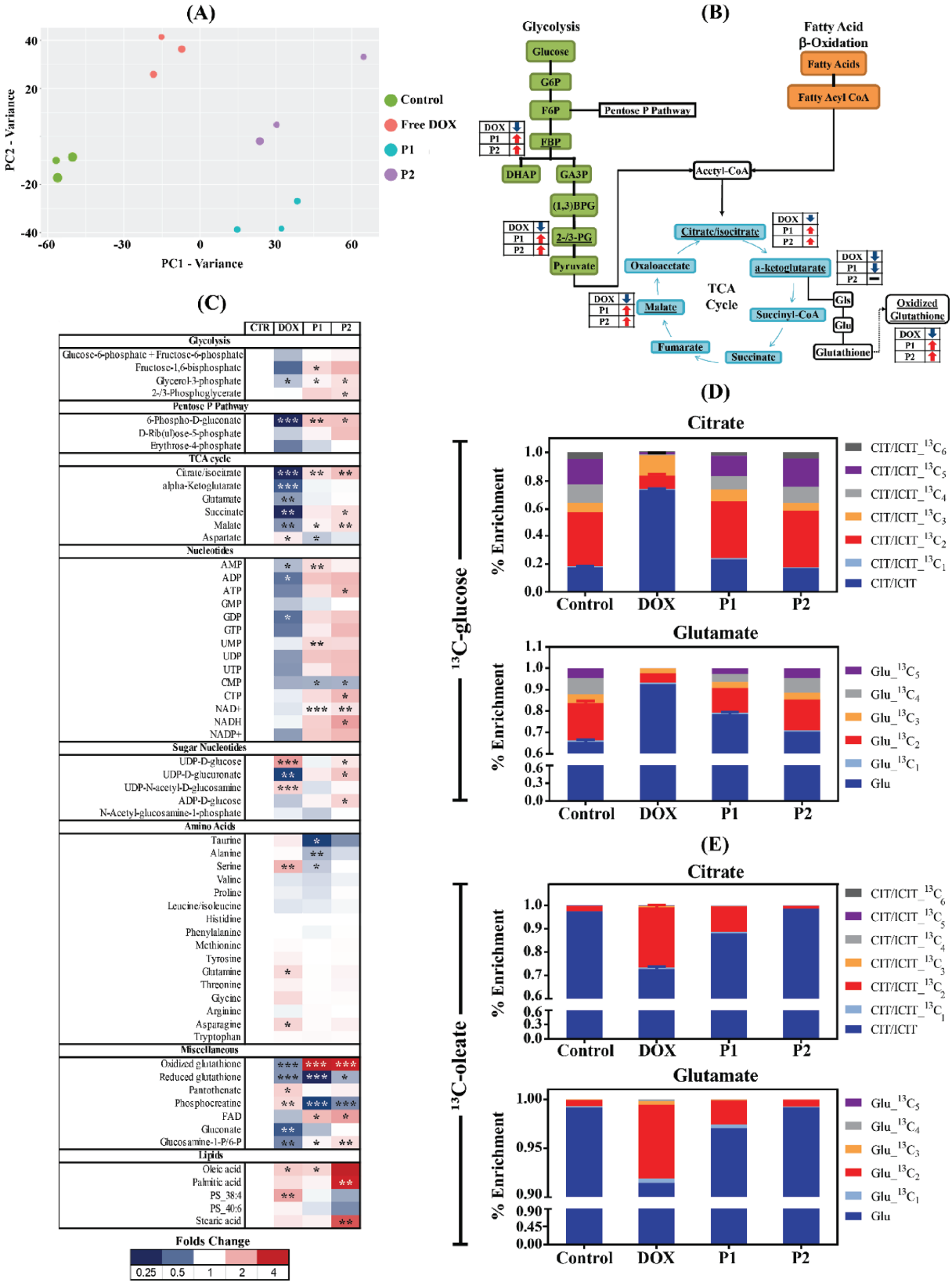

Figure 7. Metabolic response of cells treated by P1/P2 versus free DOX. Untargeted metabolomics analysis and relative flux using stable isotope tracers were used to assess metabolic changes associated with either free DOX or P1/P2 treatment. Targeted analysis shows distinct differences between metabolites of key pathways based on treatment type, as indicated by A) principle component analysis, B) changes within glycolysis and the

leads to recognizable difference in kinetics of drug release, drug metabolism, and associated intracellular activity. For example, Greco et al. observed stark differences in the release and activity of DOX against breast cancer cells when singly loaded onto a N-(2-Hydroxypropyl)methacrylamide (HPMA) polymer or loaded in combination with aminoglutethimide due to differences in the enzymes involved in drug release between the two HPMA–DOX conjugates.[66] Similarly, we hypothesize that azoreductase enzymes responsible for DOX release from P1 and P2 conjugates may impact not only the release kinetics but also intracellular metabolism of the released DOX molecules. Our current focus is on elucidating the mechanism of DOX intracellular release from P1 and P2 and its metabolism compared to free DOX.

2.6. Effect of P1 and P2 Conjugates on HepG2 Metabolic Pathways

We extended our metabolomics analysis to measure the metabolic response induced by P1 and P2 conjugates compared to free DOX treatment using an untargeted metabolomics approach and also by determining relative flux using stable isotope tracers. Principle component analysis of all features detected by untargeted analysis showed clear clustering within each treatment type and clear distinctions between each group, which indicates different metabolic profiles induced by each treatment (**Figure 7**, Panel A). Targeted analysis of major biochemical pathways such as central carbon metabolism showed clear distinctions between DOX-treated and P1/P2-treated cells (Figure 7, Panels B and C). Figure 7 Panel B identifies the differences in the presence of key markers of glycolysis and the TCA cycle based on either DOX or P1/P2 treatment. Most notably, metabolites involved in glycolysis and the TCA cycle are reduced two- to fourfold in DOX-treated cells while they are almost all upregulated up to twofold greater in P1- and P2-treated cells. Similar metabolic changes induced by free DOX have been described before[67,68] where glycolysis was reduced as well as protein, purine, pyrimidine, and glutathione biosynthesis. The inhibition of glycolysis most probably increased the oxidation of substrates other than glucose to increase ATP generation for cell survival after DOX damage.[69] In comparison, P1 and P2 conjugates induced increases in markers of glycolysis such as fructose 1,6-bisphosphate and the TCA cycle intermediates such as citrate (Figure 7, Panel B). We hypothesize that the increase in glycolysis is a response to oxidative stress caused by the generation of ROS, a primary mechanism of DOX and DOX-metabolite toxicity.[70,71] This is supported by several studies correlating increased glycolysis with oxidative stress and mitochondrial dysfunction.[72–74] Wu and Wei in their work showed increased glycolytic flux was a result of oxidative stress in skin fibroblasts from patients with myoclonic epilepsy and ragged-red fiber syndrome, in an attempt to generate NADH to help mitigate ROS generation.[72] Valbuena et al. verified the increase in glycolysis and TCA cycle was a result of poor adaptation to ROS generated in amyotrophic lateral sclerosis neuronal cells, and was a sign of neuronal death.[73] Further, plasma from patients with Alzheimer's disease, a neurodegenerative disorder associated with increased oxidative stress, caused mitochondrial dysfunction and increased glycolysis as a compensatory action, ultimately leading to a loss of cell viability, as studied by Jayasena et al.[74] Therefore, our data may suggest that the delivery of TCM F1 and D1 moieties causes high oxidative stress leading to upregulation of glycolysis and the TCA cycle and may be the primary mechanism of toxicity observed with P1 and P2 conjugates. This also explains the three- to fivefold increase in oxidized glutathione (glutathione disulfide; GSSG) present in P1/P2-treated cells (Figure 7, Panel B), which is normally upregulated to scavenge ROS.[71] Further examination of ROS presence and mitochondrial function will elucidate whether this is indeed the phenomenon at play.

To compensate for reduced glycolysis, it has been established that DOX-treated cells increase fatty acid oxidation upon treatment.[75] To further investigate the effect of different substrates on the relative utilization of fatty acid and glucose, we applied the stable isotope tracer strategy. We treated cells with DOX, P1, or P2 for 12 h, followed by a 4 h incubation with 10×10^{-3} M U-^{13}C glucose and 100×10^{-6} M oleate or 10×10^{-3} M unlabeled glucose with 100×10^{-6} M U-^{13}C oleate. We found reduced incorporation of ^{13}C glucose in citrate and glutamate metabolites for free DOX-treated cells (Figure 7, Panel D), confirming the reduced glucose flux through glycolysis. On the other hand, citrate and glutamate enrichment was not altered by P1 and P2 conjugates compared to control cells upon adding U-^{13}C glucose. This suggests that P1/P2 achieved minimal inhibition on glucose utilization. Further, free DOX shifted the TCA cycle substrate utilization toward fatty acid oxidation instead of glucose oxidation, as expected. This is evident by the increased incorporation of ^{13}C carbons from oleate in citrate and glutamate metabolites (Figure 7, Panel E). In comparison, P1 increased fatty acid oxidation more than the control or P2 conjugates but less than free DOX (Figure 7, Panel E). While the reason for the differences in fatty acid oxidation caused by either P1 or P2 remains to be identified, it is evident that the metabolic response induced by the conjugates is significantly different from that caused by free DOX, particularly in terms of the effect on glucose and fatty acid oxidation.

These results suggest that G5-mediated delivery of DOX alters both its intracellular release and the associated cellular response. To the best of our knowledge, this is the first report establishing a relationship between the mode of delivery of a chemotherapeutic cargo using a polymeric carrier and the associated intracellular release, metabolism, and effect on metabolic

TCA cycle, and C) in the heatmap of various metabolic markers. Further, using ^{13}C-glucose or ^{13}C-oleate media, we found that D) free DOX reduces glycolysis while P1 and P2 cause an increase in glycolysis, as shown in the normalized enrichment levels of citrate and glutamate in the presence of U-^{13}C glucose media. Results also show that E) free DOX increases fatty acid oxidation while P1 and P2 have little to no effect on it, as seen by the normalized enrichment of citrate and glutamate in the presence of U-^{13}C oleate media. Targeted analysis and flux tracing results are presented as the mean of three replicates ± SEM. Two-tailed Student's t-tests were used to determine the statistical difference between DOX-, P1-, or P2-treated cells compared to untreated (control) cells and are denoted by * for $P < 0.05$, ** for $P < 0.01$, and *** for $P < 0.001$.

pathways. We believe this warrants more attention and analysis of the intracellular fate of the therapeutic cargo delivered using different carriers (e.g., nanoparticles, antibodies) to establish a robust correlation between intracellular concentration-versus-time profiles. Such insight would allow accurate determination of the anticipated therapeutic response in vitro and in preclinical animal models, which will facilitate clinical translation of these technologies.

3. Conclusion

We report the synthesis and in vitro validation of a nanoparticle-based drug delivery method aimed at improving the treatment of hepatocellular carcinoma. We synthesized NAcGal$_\beta$-targeted, DOX-loaded G5 PAMAM dendrimers (e.g., NAcGal$_\beta$-PEG*c*-G5-L(x)-DOX conjugates) in two different formulations based on our previous work, P1 or P2. We verified the biocompatibility of the two conjugates and showed that they achieved efficient internalization into hepatic cancer cells, which corresponded with controllable anticancer activity comparable to free DOX. We employed metabolomics to identify that P1 and P2 conjugates deliver DOX metabolites different than DOX delivered freely in solution, indicating differences in intracellular release of the drug based on the delivery method. Further, we established that the difference in delivered DOX metabolites also induced different metabolic responses within the treated cells. Despite alternate metabolomics profiles, our results indicate that P1 and P2 conjugates present viable nanoparticle-based delivery systems that can be used for controllable doxorubicin delivery to hepatic cancer tissue.

4. Experimental Section

Materials: G5-$(NH_2)_{128}$ dendrimers with a diaminobutane core were purchased from Andrews ChemServices (Berrien Springs, MI) and purified by dialysis against deionized water using Slide-A-Lyzer dialysis cassettes (MWCO 10 kDa, Thermo Fisher Scientific, Rockford, IL) to remove imperfect dendrimers and debris. Doxorubicin-HCl was purchased from AvaChem Scientific (San Antonio, TX). *N*-acetylgalactosamine, 4-pentynoic acid, pyridine, trimethylphosphine solution (1.0 M in tetrahydrofuran), triethylamine, acetic anhydride (Ac_2O), 1-ethyl-3-(3-dimethylaminopropyl) carbodiimide hydrochloric acid (EDC.HCl), benzotriazol-1-ol (HOBt), trifluoroacetic acid (TFA), bathophenanthroline sulfonated sodium salt (SBP), copper bromide (CuBr), anhydrous dimethylsulfoxide (DMSO), anhydrous dichloromethane (DCM), anhydrous dimethylformamide (DMF), anhydrous tetrahydrofuran (THF), *cis*-aconitic anhydride (*cis*-Ac), and BSA were purchased from Sigma-Aldrich Inc. (St. Louis, MO). Trimethylsilyl trifluoromethanesulfonate, *N*,*N*-diisopropyl ethyl amine (DIPEA), camphor sulfonic acid (CSA), sodium azide (NaN_3), sodium ascorbate, and benzotriazol-1-yl-oxytripyrrolidinophosphonium hexafluorophosphate (PyBOP) were purchased from Across Organics Chemicals (Geel, Belgium). *N*-hydroxysuccinimide-poly(ethylene glycol)-Boc (2 kDa) was purchased from JenKem Technology USA Inc (Plano, TX). 2-{2-(2-Chloroethoxy)ethoxy}ethanol was purchased from TCI America (Portland, OR). Dialysis cassettes (MWCO 1–10 kDa) were purchased from Thermo Fisher Scientific (Rockford, IL). Minimum essential medium (MEM), OPTI-MEM reduced serum medium, fetal bovine serum (FBS), 0.25% trypsin/0.20% ethylenediaminetetraacetic acid (EDTA) solution, PBS, penicillin/streptomycin/amphotericin solution, sodium pyruvate, minimum nonessential amino acid solution, and 0.4% trypan blue solutions were purchased from Life Technologies (Thermo Fisher Scientific, Rockford, IL).

Spectra for Synthesis of Conjugates: Complete NMR and time-of-flight matrix-assisted laser desorption/ionization (MALDI-TOF) spectra confirming the structural identity and composition of NAcGal-*c*PEG-G5-L(x)-DOX (P1 and P2) conjugates can be found in the Supporting Information. Control particles were either purchased commercially (unmodified, cationic G5-$(NH_2)_{128}$ dendrimers) or synthesized according to the established protocols[18,76] (acetylated G5 (G5-$(Ac)_{128}$) and non DOX-loaded (NAcGal$_\beta$-PEG*c*)$_{12.1}$-G5 conjugates (P0)).

Synthesis of NAcGal-cPEG-G5-(NH$_2$)-Alkyne: The authors chose a similar approach to the previously published strategies in order to synthesize PEGylated, NAcGal-targeted G5 conjugates (Figure 2).[19,23] Briefly, D-galactosamine was treated with Ac_2 and Py to obtain D-galactopentaacetate (**1**), which was treated with trimethylsilyl trifluoromethanesulfonate (TMSOT) in DCM to obtain an oxazolidine derivative (compound **2**). The oxazolidine was reacted with an alcohol (compound **3**) in the presence of D-10-CSA in DMSO at 40 °C to yield compound **4**. The azide functional group of compound **4** was reduced to an amine with Me_3P and THF to obtain compound **5**, which facilitates coupling to the hetero bi-functional PEG with an N-hydroxysuccinimide (NHS)-activated COOH group. This peptide coupling was facilitated by EDC.HCl, HOBt, and DIPEA in DMF to obtain a PEG derivative (**6**) having NAcGal$_\beta$ at one end and on the other end a Boc-protected NH_2. The Boc group was deprotected by acid hydrolysis using TFA and DCM to unmask the terminal amine group (**7**), which was reacted with *cis*-aconitic anhydride to form the corresponding acid compound **8**. This acid was further treated with NaOMe in methanol to deprotect the *O*-acetate groups from galactosamine to obtain acid **9**. The authors attached NAcGal-functionalized NAcGal$_\beta$-PEG chains (**9**) to G5 by reacting the *cis*-aconitic acid at the PEG end with alkyne-G5-NH_2 (**10**), which was synthesized via a peptide coupling reaction between G5-$(NH_2)_{128}$ dendrimers and 4-pentynoic acid in the presence of PyBOP and DIPEA in DMSO. The primary amine groups of G5 form peptide bonds with *cis*-aconityl acids in the presence of EDC.HCl and HOBt in 6.0 pH phosphate buffer solution to obtain conjugate **11** (Figure 2).

Click Coupling of L(x)-DOX Conjugates: The authors synthesized NAcGal-cPEG-G5-L(x)-DOX conjugates by using a modified version of a standard click coupling procedure between conjugate **11** and L3/L4-DOX linkages following published protocols (Figure 2).[23] In brief, sodium ascorbate, SBP, and Cu (I) were dissolved in 3 mL of a THF:water mixture (1:1) and bubbled with argon for 10 min to obtain an oxygen-free catalyst solution. This solution was heated to 75 °C for 3–4 min, resulting in a change in solution color to brick red, and then cooled to room temperature. In a separate flask, compound **11** (1 equivalent) and L3-DOX or L4-DOX (12 equivalents) were dissolved in a THF:water mixture (1:1) and bubbled with argon for 10 min. The catalyst solution was then added to this flask by a syringe under argon gas. The whole mixture was stirred slowly (≈400 rpm) in the dark for 48 h at room temperature. The reaction mixture was then purified by dialysis against deionized water (10 kDa MWCO) for 2 d to obtain pure [(NAcGal$_\beta$-PEG*c*)$_{16.6}$-G5-(L3-DOX)$_{11.6}$] (P1) or [(NAcGal$_\beta$-PEG*c*)$_{16.6}$-G5-(L4-DOX)$_{13.4}$] (P2) conjugates dispersed in DI water (Figure 2). To obtain the concentration of these conjugates, the authors lyophilized 1 mL of the particle solution and weighed the amount of dried conjugate remaining.

Characterization of P1 and P2 Conjugates: The authors measured the particle size of the nanoparticle formulations by DLS using a 90Plus particle size analyzer (Brookhaven Instruments, Holtsville, NY). The nanoparticle solution was diluted in DI water at 1:20 v/v with 10% Tween 20 in order to limit nanoparticle aggregate formation. After sonication for 20 min, P1 and P2 conjugates were sterile-filtered through syringe filters with a pore size of 800 nm and warmed to 37 °C before measurements. Raw distribution data was plotted in Graphpad Prism software and fit using a Gaussian curve, with the mean being taken as the particle size for that replicate. The average of three separate replicates was taken to find the mean particle size ± standard error of the mean (SEM). The

authors also determined the zeta potential of the conjugates using a 90Plus Zeta Potential Analyzer (Brookhaven Instruments, Holtsville, NY). Particle formulations were dissolved in DI water at 1:20 v/v and warmed to 37 °C before analysis. The average of three separate replicates was taken to find the mean zeta potential ± SEM.

Hemolysis Assay: The authors measured the extent of erythrocyte lysis caused by P1 and P2 conjugates using the RBCs hemolysis assay.[42,77] Briefly, the authors collected fresh blood from healthy human volunteers following IRB-approved protocols into EDTA-coated tubes and immediately centrifuged them at 3000 RPM for 5 min to precipitate out the RBCs. The supernatant was removed, and a 0.15 M NaCl wash solution was used to bring the RBCs up to the initial volume of blood. The sample was spun again at 3000 RPM for 5 min, the supernatant removed, and the RBCs resuspended to the original volume. This cycle was repeated a third time before splitting the resuspended RBCs into three different EDTA-coated centrifuge tubes. These tubes were centrifuged at 3000 RPM for 5 min, and the level of the fluid was marked before removing the supernatant. PBS (1×, Gibco) was then added up to the original volume, and this solution was diluted 1:9 (v/v) in PBS to create the working stock solution. 200 µL of this working stock solution was added to each test tube, and treatment solutions of 1× PBS (negative control), DI water (positive control), 240×10^{-9} M naked G5-$(NH_2)_{128}$ dendrimers, or 240×10^{-9} M G5-equivalent of either P1 (2.78×10^{-6} M DOX) or P2 (3.22×10^{-6} M DOX) conjugates were added to the wells to achieve a final volume of 1 mL. The samples were incubated for 1 h at 37 °C and then mixed by inversion and centrifuged at maximum speed for 5 min. Finally, 200 µL of the supernatant was collected and added to 96-well plates, and the excitation of hemoglobin was measured by UV (λ_{ex} = 541 nm). The raw data was normalized to PBS values (which is nonhemolytic due to its buffering capacity[35]) and presented as a percentage of hemolysis caused by DI water (which causes hemolysis through osmotic swelling and rupture of RBCs[35]). Results are presented as the mean of three replicates ± SEM.

Platelet Aggregation: The authors evaluated the interaction of platelets with P1 and P2 conjugates using light transmission platelet aggregometry according to published protocols.[42] Briefly, fresh blood was isolated from anesthetized C57BL/6 mice via cardiac puncture using 20 gauge needles flushed with 3.2% sodium citrate and was diluted 1:1 v/v with HEPES Tyrode (HT) buffer and centrifuged at $50 \times g$ for 10 min at room temperature. The supernatant was collected as platelet rich plasma (PRP), and the precipitate was resuspended in HT buffer up to the original volume and spun again at $50 \times g$ for 10 min at room temperature. The supernatant was collected and added to the original PRP fraction, while the precipitate was resuspended with HT buffer to the original volume. After spinning the suspension at $1200 \times g$ for 10 min at room temperature, the supernatant was collected into a separate tube as the platelet poor plasma (PPP) fraction. The authors mixed either naked G5-$(NH_2)_{128}$ dendrimers, P0, P1, or P2 conjugates with 500 µL of PRP solution prewarmed to 37 °C to achieve a final G5-equivalent concentration of 240×10^{-9} M. The authors monitored platelet aggregation over 10 min using the Aggro-Link data reduction system (Chrono-log Corporation, Havertown, PA). The authors also measured the platelet aggregation of 500 µL PRP incubated with PBS or 10×10^{-6} M ADP as negative or positive controls, respectively. Results are presented as the mean of three replicates ± SEM.

Opsonization by Serum Proteins: The authors also assessed the extent of particle opsonization by measuring the binding of BSA as a model protein to P1 and P2 conjugates as a function of particle composition and time, based on published protocols.[18] Briefly, the authors prepared G5-$(NH_2)_{128}$, $(NAcGal_{\beta}\text{-}PEG_c)_{12.1}$-G5 (**P0**), P1, and P2 conjugates in warmed PBS (pH 7.4) at a particle concentration of 241×10^{-9} M. Conjugates were mixed with BSA (0.2 mg mL^{-1}) in a quartz cuvette and incubated at 37 °C for 60 min. The fluorescence of BSA tryptophan residues (λ_{ex}: 280 nm; λ_{em} scanned between 300 and 400 nm) was measured at time zero (I^0) and at different incubation times (I) up to 60 min in a QM4 fluorescence spectrophotometer (Perkin-Elmer, Waltham, MA). The authors divided the initial BSA fluorescence (I^0) by the measured fluorescence at different timepoints (I) to evaluate the extent of BSA quenching, as an indication of BSA binding to the particle's surface, indicated by $I^0/I > 1$. BSA adsorption to each particle was measured in triplicates and presented as the mean $I^0/I \pm$ SEM. Statistical comparisons were made between the I^0/I values measured for conjugates and that observed with BSA alone using student's t-test.

Cell Culture: HepG2 and Hep3B cells were cultured in T-75 flasks using MEM supplemented with 10% FBS, 1% antibiotic-antimycotic, 1% sodium pyruvate, 1% nonessential amino acids, and 1 mL gentamicin. HepG2 and Hep3B cells were maintained at 37 C, 5% CO_2, and 95% relative humidity and medium was changed every 48 h. The cells were passaged at 80%–90% confluency using a 0.25% trypsin/0.20% EDTA solution.

Uptake of P1 and P2 Conjugates into Hepatic Cancer Cells: The internalization of P1 and P2 conjugates into HepG2 and Hep3B cells was measured as a function of particle composition and concentration via flow cytometry. Briefly, 250 000 HepG2 or Hep3B cells were seeded in 24-well plates and allowed to adhere overnight. Treatment solutions of P1 or P2 conjugates ($7–285 \times 10^{-9}$ M G5 concentration; $100–4000 \times 10^{-9}$ M NAcGal concentration) were prepared in OPTI-MEM and then incubated with the cells for 2 h at 37 °C. The authors used free DOX treatments for comparison and included them at concentrations equivalent to the DOX loaded onto either P1 or P2 conjugates. The authors also used cells treated only with OPTI-MEM as a control. After removing the treatment medium and washing the cells with warmed PBS twice, the adherent cells were removed from the plates using a 0.25% trypsin/0.20% EDTA solution and then suspended in fresh culture medium. The cells were then transferred to flow cytometry tubes, centrifuged at 1000 RPM for 5 min at 4 °C, kept on ice, and then resuspended immediately before analysis. Samples were analyzed by flow cytometry using the intrinsic fluorescence of DOX (λ_{ex}: 488 nm; λ_{em}: 613 nm) on a Beckman Coulter Cyan ADP instrument provided by the Flow Cytometry Core at the University of Michigan (Ann Arbor, MI). Data is presented as the mean ± SEM for $n = 4$ replicates, and the authors used untreated cells in blank OPTI-MEM as the negative control.

Cytotoxicity of P1 and P2 Conjugates: The cytotoxicity of P1 and P2 conjugates against HepG2 and Hep3B cells was measured as a function of DOX concentration via the clonogenic survival assay.[23] Briefly, 250 000 HepG2 or Hep3B cells were plated in T-25 flasks and allowed to adhere overnight. Treatments of free DOX, P1, or P2 conjugates were prepared at equivalent DOX concentrations ($1–10\,000 \times 10^{-9}$ M DOX) in OPTI-MEM at a total volume of 5 mL and incubated with the cells for 72 h. After the treatment period, the cells were washed twice with PBS, trypsinized with 0.25% trypsin/0.20% EDTA solution, collected into tubes, and centrifuged at 1000 RPM for 5 min. The supernatant was then aspirated and the cells were resuspended in 1 mL of fresh medium and kept on ice during counting. The cell count was established manually using a hemocytometer and were seeded into 6-well plates at either 1000 or 2000 cells per well in 3 mL of medium, with three replicates for each cell count. The cells were allowed to sit undisturbed for 14 d at 37 °C and 5% CO_2. The medium was then removed and the cells were washed with PBS once. The colonies were fixed and stained using 1 mL of a methanol/glacial acetic acid (75/25% v/v) solution with 0.04% w/v trypan blue and incubated for 15–30 min. The stain was then aspirated and the plates were allowed to dry uncovered for 20 min. The stained colonies were counted by visual inspection. Plating efficiency (PE) was determined by dividing the number of control untreated colonies resulting from the known number seeded cells (1000 or 2000). The surviving fraction of treated cells was then determined by dividing the number of counted colonies by the PE. The surviving fraction across all six replicates was averaged and presented as % survival ± SEM.

Metabolomics Analysis: To measure the intracellular release of either free DOX or P1/P2 conjugates as well as the associated metabolic response upon treatment, the authors applied metabolomics analysis on treated cells, as described previously.[78–80] For treatment, 1×10^6 HepG2 cells were seeded in 6-well plates and allowed to adhere and double in population over 24 h. Treatment solutions of free DOX (10×10^{-6} M) or P1 and P2 (10×10^{-6} M DOX-equivalent) in OPTI-MEM were incubated with the cells for 12 h. After treatment, cell plates

were rinsed with 200×10^{-3} M ammonium acetate and quenched with liquid nitrogen. Metabolites were extracted with ice cold 8:1:1 methanol:chloroform:water and assayed by high performance liquid chromatography coupled to time-of-flight mass spectrometry. For polar metabolites, chromatographic separation was performed using an Agilent Technologies (Santa Clara, CA) 1200 HPLC system equipped with a Phenomenex (Torrance, CA) Luna NH_2 HPLC column (1.0 mm inner bore × 150 mm long and packed with 3 µm particles). Mobile phase A was 100% acetonitrile and mobile phase B (MPB) was 100% 5×10^{-3} M ammonium acetate adjusted to pH 9.9 with ammonium hydroxide. The gradient started at 20% MPB and was ramped to 100% MPB over 20 min, held for 5 min, and returned to 20% MPB for an additional 7 min. Doxorubicin and its metabolites were separated using an Acquity UPLC BEH C18 column (2.1 × 100 mm, 1.7 µm) and a 2.1 × 5 mm VanGuard precolumn using the following conditions: mobile phase A of 0.1% formic acid and mobile phase B of acetonitrile with 0.1% formic acid. The gradient was started at 5% B and progressed to 100% B in 25 min followed by being held at 100% B for 10 min before reconditioning the column back to 5% B for 10 more min.

For isotope tracer studies, after the same treatment for 12 h by either free DOX, P1, or P2, the treatment media was replaced by media containing a stable isotope tracer. One medium contained 10×10^{-3} M U-^{13}C glucose and 100×10^{-6} M oleate while the other contained 10×10^{-3} M glucose and 100×10^{-6} M U-^{13}C oleate. Cells were incubated for 4 h before being quenched and analyzed for metabolites as described above.

Data Analysis and Statistics: Targeted analysis was performed to measure specific metabolites involved in central carbon metabolism such as glycolysis and TCA cycle intermediates. Untargeted analysis was performed using XCMS online.[81] Features that showed substantial differences were manually quantified and their masses were checked against both human metabolome database and METLIN.

Supporting Information

Supporting Information is available from the Wiley Online Library or from the author.

Acknowledgements

S.P.K. and G.T. contributed equally to this work. The authors would like to thank Dr. Jinsang Kim and Dr. Daniel Eitzman for providing access to their fluorescence spectrophotometer and light aggregometry instrument, respectively, as well as the Michigan Regional Comprehensive Metabolomics Resource Core (MRC2) for support with the metabolomics work (NIH Grant #U24DK097153). Sibu P. Kuruvilla recognizes the support of the NSF Graduate Research Fellowship (GRFP) award and the University of Michigan Rackham Merit Fellowship (RMF).

Received: September 12, 2016
Revised: November 25, 2016
Published online: January 13, 2017

[1] A. G. Singal, J. A. Marrero, *Curr. Opin. Gastroenterol.* **2010**, *26*, 189.
[2] J. Ferlay, I. Soerjomataram, M. Ervik, R. Dikshit, S. Eser, C. Mathers, M. Rebelo, D. M. Parkin, D. Forman, F. Bray, *GLOBOCAN 2012 v1.0, Cancer Incidence and Mortality Worldwide: IARC CancerBase*, Vol. no. *11* [Internet], International Agency for Research on Cancer, Lyon, France **2013**, http://globocan.iarc.fr/Pages/fact_sheets_cancer.aspx (accessed: December 13, 2016).
[3] A. G. Singal, H. B. El-Serag, *Clin. Gastroenterol. Hepatol.* **2015**, *13*, 2140.
[4] H. B. El-Serag, *Hepatol. Res.* **2007**, *37*, S88.
[5] J. L. Petrick, S. P. Kelly, S. F. Altekruse, K. A. McGlynn, P. S. Rosenberg, *J. Clin. Oncol.* **2016**, *34*, 1787.
[6] D. Miyaki, H. Aikata, Y. Honda, N. Naeshiro, T. Nakahara, M. Tanaka, Y. Nagaoki, T. Kawaoka, S. Takaki, K. Waki, A. Hiramatsu, S. Takahashi, M. Ishikawa, H. Kakizawa, K. Awai, K. Chayama, *J. Gastroenterol. Hepatol.* **2012**, *27*, 1850.
[7] S. W. Shin, *Korean J. Radiol.* **2009**, *10*, 425.
[8] R. Yamada, K. Kishi, M. Sato, T. Sonomura, N. Nishida, K. Tanaka, Y. Shioyama, M. Terada, M. Kimura, *World J. Surg.* **1995**, *19*, 795.
[9] T. J. Vogl, N. N. N. Naguib, N.-E. A. Nour-Eldin, P. Rao, A. H. Emami, S. Zangos, M. Nabil, A. Abdelkader, *Eur. J. Radiol.* **2009**, *72*, 505.
[10] E. Garwood, N. Fidelman, S. Hoch, R. Kerlan Jr., F. Yao, *Liver Transplant.* **2013**, *19*, 164.
[11] I. Idilman, B. Peynircioglu, B. E. Cil, B. Doganay Erdogan, S. Yalcin, Y. Bayraktar, T. Kav, K. Altundag, F. Balkanci, *Turk. J. Gastroenterol.* **2013**, *24*, 141.
[12] H.-Y. Cheng, X. Wang, D. Chen, A.-M. Xu, Y.-C. Jia, *World J. Gastroenterol.* **2005**, *11*, 3644.
[13] K. Barnett, M. Malafa, *Int. J. Gastrointest. Cancer* **2001**, *30*, 147.
[14] A. Basile, G. Carrafiello, A. M. Ierardi, D. Tsetis, E. Brountzos, *Cardiovasc. Intervent. Radiol.* **2012**, *35*, 765.
[15] O. Fardel, E. Jigorel, M. Le Vee, L. Payen, *Biomed. Pharmacother.* **2005**, *59*, 104.
[16] V. Gajbhiye, V. K. Palanirajan, R. K. Tekade, N. K. Jain, *J. Pharm. Pharmacol.* **2009**, *61*, 989.
[17] H. Liu, H. Wang, Y. Xu, R. Guo, S. Wen, Y. Huang, W. Liu, M. Shen, J. Zhao, G. Zhang, X. Shi, *ACS Appl. Mater. Interfaces* **2014**, *6*, 6944.
[18] S. H. Medina, G. Tiruchinapally, M. V. Chevliakov, Y. Y. Durmaz, R. N. Stender, W. D. Ensminger, D. S. Shewach, M. E. H. ElSayed, *Adv. Healthcare Mater.* **2013**, *2*, 1337.
[19] S. H. Medina, V. Tekumalla, M. V Chevliakov, D. S. Shewach, W. D. Ensminger, M. E. H. El-Sayed, *Biomaterials* **2011**, *32*, 4118.
[20] H. Mu, K.-X. Lin, H. Zhao, S. Xing, C. Li, F. Liu, H.-Z. Lu, Z. Zhang, Y.-L. Sun, X.-Y. Yan, J.-Q. Cai, X.-H. Zhao, *World J. Gastroenterol.* **2014**, *20*, 5826.
[21] Y. Cao, Y. He, H. Liu, Y. Luo, M. Shen, J. Xia, X. Shi, *J. Mater. Chem. B* **2015**, *3*, 286.
[22] D. Ouyang, H. Zhang, H. S. Parekh, S. C. Smith, *Biophys. Chem.* **2011**, *158*, 126.
[23] S. H. Medina, M. V Chevliakov, G. Tiruchinapally, Y. Y. Durmaz, S. P. Kuruvilla, M. E. H. Elsayed, *Biomaterials* **2013**, *34*, 4655.
[24] A. R. Nicholas, M. J. Scott, N. I. Kennedy, M. N. Jones, *Biochim. Biophys. Acta* **2000**, *1463*, 167.
[25] S. Kaufman, O. Borisov, M. Textor, E. Reimhult, *Soft Matter* **2011**, *7*, 9267.
[26] S. Honary, F. Zahir, *Trop. J. Pharm. Res.* **2013**, *12*, 265.
[27] M. Longmire, P. L. Choyke, H. Kobayashi, *Nanomedicine* **2008**, *3*, 703.
[28] H. S. Choi, W. Liu, P. Misra, E. Tanaka, J. P. Zimmer, B. Itty, M. G. Bawendi, J. V Frangioni, *Nat. Biotechnol.* **2009**, *25*, 1165.
[29] N. Bertrand, J. Wu, X. Xu, N. Kamaly, O. C. Farokhzad, *Adv. Drug Delivery Rev.* **2014**, *66*, 2.
[30] J. Fang, H. Nakamura, H. Maeda, *Adv. Drug Delivery Rev.* **2011**, *63*, 136.
[31] H. Maeda, G. Y. Bharate, J. Daruwalla, *Eur. J. Pharm. Biopharm.* **2009**, *71*, 409.
[32] R. Duncan, Y.-N. Sat-Klopsch, A. M. Burger, M. C. Bibby, H. H. Fiebig, E. A. Sausville, *Cancer Chemother. Pharmacol.* **2013**, *72*, 417.
[33] J. B. Pryor, B. J. Harper, S. L. Harper, *Int. J. Nanomed.* **2014**, *9*, 1947.
[34] S. Sadekar, H. Ghandehari, *Adv. Drug Delivery Rev.* **2012**, *64*, 571.
[35] W. Xue, Y. Feng, F. Wang, Y. Guo, P. Li, L. Wang, Y. Liu, *Sci. Rep.* **2016**, *6*, 22149.

[36] B. Klajnert, S. Pikala, M. Bryszewska, *Proc. R. Soc. A Math. Phys. Eng. Sci.* **2009**, *466*, 1527.
[37] H.-T. Chen, M. F. Neerman, A. R. Parrish, E. E. Simanek, *J. Am. Chem. Soc.* **2004**, *162*, 10044.
[38] V. Gajbhiye, P. V. Kumar, R. K. Tekade, N. K. Jain, *Curr. Pharm. Des.* **2007**, *13*, 415.
[39] W. Wang, W. Xiong, Y. Zhu, H. Xu, X. Yang, *J. Biomed. Mater. Res. Part B Appl. Biomater.* **2010**, *93*, 59.
[40] V. Gajbhiye, P. Vijayaraj Kumar, R. K. Tekade, N. K. Jain, *Eur. J. Med. Chem.* **2009**, *44*, 1155.
[41] K. Xiao, Y. Li, J. Luo, J. S. Lee, W. Xiao, A. M. Gonik, R. G. Agarwal, K. S. Lam, *Biomaterials* **2011**, *32*, 3435.
[42] O. Aydin, I. Youssef, Y. Y. Durmaz, G. Tiruchinapally, M. E. H. Elsayed, *Mol. Pharmaceutics* **2016**, *13*, 1413.
[43] D. Woulfe, J. Yang, L. Brass, *J. Clin. Invest.* **2001**, *107*, 1503.
[44] A. Radomski, P. Jurasz, D. Alonso-Escolano, M. Drews, M. Morandi, T. Malinski, M. W. Radomski, *Br. J. Pharmacol.* **2005**, *146*, 882.
[45] D. E. Owens, N. A. Peppas, D. E. Owens III, N. A. Peppas, *Int. J. Pharm.* **2006**, *307*, 93.
[46] S. M. Moghimi, J. Szebeni, *Prog. Lipid Res.* **2003**, *42*, 463.
[47] F. Fu, Y. Wu, J. Zhu, S. Wen, M. Shen, X. Shi, *ACS Appl. Mater. Interfaces* **2014**, *6*, 16416.
[48] O. Khorev, D. Stokmaier, O. Schwardt, B. Cutting, B. Ernst, *Bioorg. Med. Chem.* **2008**, *16*, 5216.
[49] B. Thapa, P. Kumar, H. Zeng, R. Narain, *Biomacromolecules* **2015**, *16*, 3008.
[50] C. H. Wu, G. Y. Wu,*Gastroenterology* **1998**, *114*, 1304.
[51] A. Shiber, W. Breuer, T. Ravid, *Prion* **2014**, *8*, 276.
[52] L. Y. Chan, B. A. Sc, E. K. F. Yim, D. Ph, A. B. H. Choo, *Tissue Engineering Part C: Methods* **2013**, *19*, 156.
[53] A. L. Schwartz, S. E. Fridovich, B. B. Knowles, H. F. Lodish, *J. Biol. Chem.* **1981**, *256*, 8878.
[54] Y. Li, G. Huang, J. Diakur, L. I. Wiebe, *Curr. Drug Delivery* **2008**, *5*, 299.
[55] T. K.-W. Lee, T. C.-M. Lau, I. O.-L. Ng, *Cancer Chemother. Pharmacol.* **2002**, *49*, 78.
[56] H. S. Yoo, K. H. Lee, J. E. Oh, T. G. Park, *J. Controlled Release* **2000**, *68*, 419.
[57] R. Liu, D. Li, B. He, X. Xu, M. Sheng, Y. Lai, G. Wang, Z. Gu, *J. Controlled Release* **2011**, *152*, 49.
[58] F. Capone, E. Guerriero, A. Sorice, G. Colonna, G. Storti, J. Pagliuca, G. Castello, S. Costantini, *Sci. World J.* **2014**, *2014*, 450390.
[59] R. D. Arnold, J. E. Slack, R. M. Straubinger, *J. Chromatogr. B* **2004**, *808*, 141.
[60] E. L. Westman, M. J. Canova, I. J. Radhi, K. Koteva, I. Kireeva, N. Waglechner, G. D. Wright, *Chem. Biol.* **2012**, *19*, 1255.
[61] D. Kaushik, G. Bansal, *J. Pharm. Anal.* **2015**, *5*, 285.
[62] M. Mondon, B. Renoux, P. Martin, B. Pfeiffer, P. Renard, A. Pierre, *Bioorg. Med. Chem.* **2002**, *10*, 253.
[63] M. Gan, B. Liu, Y. Tan, Q. Wang, H. Zhou, H. He, Y. Ping, Z. Yang, Y. Wang, C. Xiao, *J. Nat. Prod.* **2015**, *78*, 2260.
[64] P. G. Guilfoile, C. R. Hutchinson, *J. Bacteriol.* **1992**, *174*, 3651.
[65] M. J. H. Janssen, D. J. A. Crommelin, G. Storm, A. Hulshoff, *Int. J. Pharm.* **1985**, *23*, 1.
[66] F. Greco, M. J. Vicent, S. Gee, A. T. Jones, J. Gee, R. I. Nicholson, R. Duncan, *J. Controlled Release* **2007**, *117*, 28.
[67] B. Cao, M. Li, W. Zha, Q. Zhao, R. Gu, *Metabolomics* **2013**, *9*, 960.
[68] K. Kim, J. Yang, S. Jun, H. Sik, D. Hyun, Y. Kim, J. Yun, D. Soo, S. Min, *J. Appl. Toxicol.* **2013**, *33*, 1251.
[69] M. N. Triba, A. Starzec, N. Bouchemal, E. Guenin, G. Y. Perret, L. Le Moyec, *NMR Biomed.* **2010**, *23*, 1009.
[70] K. Wu, I. Kryczek, L. Chen, W. Zou, T. H. Welling, *Cancer Res.* **2009**, *69*, 8067.
[71] Y. Song, R. Zhao, Y. Hu, F. Hao, N. Li, G. Nie, H. Tang, Y. Wang, *J. Proteome Res.* **2015**, *14*, 5193.
[72] S. B. Wu, Y. H. Wei, *Biochim. Biophys. Acta, Mol. Basis Dis.* **2012**, *1822*, 233.
[73] G. N. Valbuena, M. Rizzardini, S. Cimini, A. P. Siskos, C. Bendotti, L. Cantoni, H. C. Keun, *Mol. Neurobiol.* **2015**, *53*, 2222.
[74] T. Jayasena, A. Poljak, N. Braidy, G. Smythe, M. Raftery, M. Hill, H. Brodaty, J. Trollor, N. Kochan, P. Sachdev, *PLoS One* **2015**, *10*, 1.
[75] Q. Niu, Z. Li, G. Du, X. Qin, *J. Pharm. Biomed. Anal.* **2016**, *118*, 338.
[76] S. H. Medina, M. E. H. El-Sayed, *Chem. Rev.* **2009**, *109*, 3141.
[77] Y. L. Lin, G. Jiang, L. K. Birrell, M. E. H. El-Sayed, *Biomaterials* **2010**, *31*, 7150.
[78] M. El-Azzouny, C. R. Evans, M. K. Treutelaar, R. T. Kennedy, C. F. Burant, *J. Biol. Chem.* **2014**, *289*, 13575.
[79] M. A. Lorenz, M. A. El Azzouny, R. T. Kennedy, C. F. Burant, *J. Biol. Chem.* **2013**, *288*, 10923.
[80] M. A. ElAzzouny, C. R. Evans, C. F. Burant, R. T. Kennedy, *PLoS One* **2015**, *10*, 1.
[81] R. Tautenhahn, G. J. Patti, D. Rinehart, G. Siuzdak, *Anal. Chem.* **2012**, *84*, 5035.